

Young star clusters in the outer disks of LITTLE THINGS dwarf irregular galaxies

Deidre A. Hunter¹, Bruce G. Elmegreen², Elizabeth Gehret¹

ABSTRACT

We examine *FUV* images of the LITTLE THINGS sample of nearby dwarf irregular (dIrr) and Blue Compact Dwarf (BCD) galaxies to identify distinct young regions in their far outer disks. We use these data, obtained with the *Galaxy Evolution Explorer* satellite, to determine the furthest radius at which *in situ* star formation can currently be identified. The *FUV* knots are found at distances from the center of the galaxies of 1 to 8 disk scale lengths and have ages of ≤ 20 Myrs and masses of $20 M_{\odot}$ to $1 \times 10^5 M_{\odot}$. The presence of young clusters and OB associations in the outer disks of dwarf galaxies shows that dIrrs do have star formation taking place there in spite of the extreme nature of the environment. Most regions are found where the H I surface density is $\sim 1 M_{\odot} \text{ pc}^{-2}$, although both the H I and dispersed old stars go out much further. This limiting density suggests a cutoff in the ability to form distinct OB associations and perhaps even stars. We compare the star formation rates in the *FUV* regions to the average rates expected at their radii and beyond from the observed gas, using the conventional correlation for gas-rich regions. The localized rates are typically 10% of the expected average rates for the outer disks. Either star formation in dIrrs at surface densities $< 1 M_{\odot} \text{ pc}^{-2}$ occurs without forming distinct associations, or the Kennicutt-Schmidt relation over-predicts the rate beyond this point. In the latter case, the stellar disks in the far-outer parts of dIrrs result from scattering of stars from the inner disk.

Subject headings: galaxies: irregular — galaxies: star formation

1. Introduction

Star formation in dwarf irregular galaxies (dIrrs) is difficult to understand because gas densities are low, but this is particularly true in the outer parts where the gas densities

¹Lowell Observatory, 1400 West Mars Hill Road, Flagstaff, Arizona 86001 USA

²IBM T. J. Watson Research Center, PO Box 218, Yorktown Heights, New York 10598 USA

are even lower than in the central regions. There, the standard 2-dimensional Toomre (1964) gravitational instability parameter for the gas, suggested by Kennicutt (1989) as an important parameter for star formation, predicts that the gas is highly stable against collapse into star-forming clouds (Hunter et al. 2011). Yet, *FUV* emission, a signpost of recent star formation, is detected even into the outer disks.

In a deep-imaging study, we obtained *V*-band and *Galaxy Evolution Explorer* (*GALEX*; Martin et al. 2005) *FUV* images of 4 dIrr galaxies and one Blue Compact Dwarf (BCD), and *B*-band images for 3 of the dIrrs (Hunter et al. 2011). Through surface photometry we traced stellar disks in these images to $\mu_V \sim 30$ mag arcsec⁻². We found that the stellar surface brightness in both *V* and *FUV* continues exponentially as far out as we can measure (see also Bellazzini et al. 2014). The presence of *FUV* emission into the outer disk suggests a continuity of star formation with radius even though the outer gas is stable against two-dimensional gravitational collapse in the conventional model (Elmegreen & Hunter 2015).

In spiral galaxies, numerical simulations show that spiral arms are capable of scattering stars into the outer disks (Roškar et al. 2008; Minchev et al. 2012; Radburn-Smith et al. 2012), and this could be a significant source of the stellar populations there. However, dIrrs do not have spiral arms. Are outer disks of dIrrs populated primarily through stars scattered from the inside out or from *in situ* star formation? Are the outer parts of dIrrs from halos and not disks (Martin-Navarro et al. 2014)? If star formation is taking place in the outer parts of dIrrs, then there should be young *FUV*-bright star clusters, not just diffuse *FUV* emission. We have previously identified clusters and associations to a radius of a few disk scale lengths (Melena et al. 2009). Here we use *FUV* images to search for young star clusters and OB associations in the far outer regions of a larger sample of nearby dIrr galaxies. Since scattering takes longer than the ages of young clusters and strong scattering may destroy clusters (but see Carraro et al. 2006), this search is a good test for *in situ* star formation in outer disks.

We also examine the environments for star formation in the far outer parts of these galaxies (§4). The pressure and average density are low, gravity is weak, and the dynamical time is long. Most of the identified regions occur near the radius where the average gas surface density drops below $\sim 1 M_\odot \text{ pc}^{-2}$, suggesting a cutoff or slowdown at lower densities. The gas and distributed stellar population go further than this. To test whether the outer disk might be built up from dispersed regions like those we observe, we compare in §5 the star formation rates (SFRs) in the *FUV* regions to the average rates expected in the outer disks from the Kennicutt-Schmidt relation (Kennicutt & Evans 2012).

2. Sample, Data, and Procedure

The sample of galaxies is taken from LITTLE THINGS (Local Irregulars That Trace Luminosity Extremes, The H I Nearby Galaxy Survey, Hunter et al. 2012). This is a multi-wavelength survey of nearby (< 10.3 Mpc) dIrr galaxies and Blue Compact Dwarfs (BCDs), which builds on the THINGS project, whose emphasis was on nearby spirals (Walter et al. 2008). The galaxies and a few key parameters are listed in Table 1. The galaxies Haro 29, Haro 36, Mrk 178, and VIIZw 403, which appear at the end of the table, are classified as BCDs. NGC 3738, classified as a dIrr, has characteristics, such as a central concentration of stars, star formation, and gas, that are similar to BCDs, and so we will include it with the BCDs when that group is singled out.

The LITTLE THINGS sample was chosen to be relatively isolated because we are investigating internal processes of star formation. None of the galaxies are companions to large spiral galaxies, members of dense clusters, or obviously engaged in an interaction with another galaxy. Most are, however, members of groups and so other galaxies are around. In addition a few galaxies and particularly the BCDs (NGC 1569, IC 10, Haro 29, Haro 36, Mrk 178, VIIZw 403) are undergoing bursts of star formation that may have been triggered by some sort of external process, including mergers (Nidever et al. 2013; Ashley et al. 2013, 2014). Hunter & Elmegreen (2004) gives the nearest neighbor to each galaxy and their separation. The non-starburst LITTLE THINGS galaxies are 110-1100 kpc from their nearest known neighbor, with a median separation of 480 kpc. The starburst sub-sample is at a comparable range of distances – 240-900 kpc with a median separation of 450 kpc. Therefore, we expect that for most of the galaxies the extra-galactic environment is not a factor in determining the extent of star-formation in the systems.

We used FUV (1516 Å) images obtained by *GALEX* (Melena et al. 2009; Hunter et al. 2010, 2011; Zhang et al. 2012) to identify knots of emission in the outer disks of each galaxy. In order to better distinguish knots from the wide-spread diffuse emission, we subtracted the stellar continuum from each FUV image using the V -band image. The FUV image was geometrically transformed to match the pixel scale and dimensions of the V -band image. The V -band image was scaled and Gaussian-smoothed so that, as well as possible, when it was subtracted from the FUV image, the diffuse emission disappeared.

In order to select FUV knots that we were confident belonged to the galaxy, we used $FUV - NUV$ false-color pictures produced by the *GALEX* pipeline to pick out bright, blue knots that stood out compared to the surrounding background/foreground populations. In particular we were looking at the density of comparably bright and blue objects well beyond the galaxy. The shape of the object is also a clue: is it resolved compared to a star or lumpy? As a training exercise, we began with a few galaxies also studied by Melena et al.

Table 1. Furthest FUV region

| Galaxy | D (Mpc) | R_D^a (kpc) | R_{Br}^b (kpc) | Furthest <i>FUV</i> region | | | | |
|-----------|------------|------------------|---------------------|----------------------------|------------------|-----------------------|----------------|-------------------|
| | | | | RA (h:m:s) | DEC (d:am:as) | R_{knot}^c (kpc) | R_{knot}/R_D | R_{knot}/R_{Br} |
| CvnIdwa | 3.6 | 0.25±0.12 | 0.56± 0.49 | 12:38:37.8 | +32:45:40 | 0.49±0.03 | 2.0± 0.9 | 0.9± 0.8 |
| DDO 43 | 7.8 | 0.87±0.10 | 1.46± 0.53 | 7:28:16.7 | +40:47:01 | 1.93±0.08 | 2.2± 0.3 | 1.3± 0.5 |
| DDO 46 | 6.1 | 1.13±0.05 | 1.27± 0.18 | 7:41:26.9 | +40:05:08 | 3.02±0.06 | 2.3± 0.1 | 2.4± 0.3 |
| DDO 47 | 5.2 | 1.34±0.05 | ... | 7:42:00.0 | +16:49:40 | 5.58±0.05 | 4.2± 0.2 | ... |
| DDO 50 | 3.4 | 1.48±0.06 | 2.65± 0.27 | 8:18:23.8 | +70:43:18 | 4.86±0.03 | 3.3± 0.1 | 1.8± 0.2 |
| DDO 52 | 10.3 | 1.26±0.04 | 2.80± 1.35 | 8:28:26.3 | +41:50:25 | 3.39±0.10 | 2.7± 0.1 | 1.2± 0.6 |
| DDO 53 | 3.6 | 0.47±0.01 | 0.62± 0.09 | 8:34:11.8 | +66:10:12 | 1.19±0.03 | 2.5± 0.1 | 1.9± 0.3 |
| DDO 63 | 3.9 | 0.68±0.01 | 1.31± 0.10 | 9:40:56.0 | +71:12:15 | 2.89±0.04 | 4.2± 0.1 | 2.2± 0.2 |
| DDO 69 | 0.8 | 0.19±0.01 | 0.27± 0.05 | 9:59:12.4 | +30:44:37 | 0.76±0.01 | 4.0± 0.2 | 2.8± 0.5 |
| DDO 70 | 1.3 | 0.44±0.01 | 0.13± 0.07 | 10:00:05.4 | +5:17:47 | 1.34±0.01 | 3.1± 0.1 | 10.3± 5.5 |
| DDO 75 | 1.3 | 0.18±0.01 | 0.71± 0.08 | 10:11:08.5 | -4:39:07 | 1.38±0.01 | 7.7± 0.4 | 1.9± 0.2 |
| DDO 87 | 7.7 | 1.21±0.02 | 0.99± 0.11 | 10:49:25.1 | +65:30:41 | 4.23±0.07 | 3.5± 0.1 | 4.3± 0.5 |
| DDO 101 | 6.4 | 0.97±0.06 | 1.16± 0.11 | 11:55:36.4 | +31:31:18 | 1.23±0.06 | 1.3± 0.1 | 1.1± 0.1 |
| DDO 126 | 4.9 | 0.84±0.13 | 0.60± 0.05 | 12:27:14.1 | +37:08:01 | 3.37±0.05 | 4.0± 0.6 | 5.6± 0.5 |
| DDO 133 | 3.5 | 1.22±0.04 | 2.25± 0.24 | 12:32:48.9 | +31:31:42 | 2.20±0.03 | 1.8± 0.1 | 1.0± 0.1 |
| DDO 154 | 3.7 | 0.48±0.02 | 0.62± 0.09 | 12:53:58.4 | +27:07:20 | 2.65±0.04 | 5.5± 0.2 | 4.3± 0.6 |
| DDO 167 | 4.2 | 0.22±0.01 | 0.56± 0.11 | 13:13:20.6 | +46:19:32 | 0.70±0.04 | 3.2± 0.2 | 1.2± 0.3 |
| DDO 168 | 4.3 | 0.83±0.01 | 0.72± 0.07 | 13:14:31.4 | +45:54:12 | 2.25±0.04 | 2.7± 0.1 | 3.1± 0.3 |
| DDO 187 | 2.2 | 0.37±0.06 | 0.28± 0.05 | 14:15:54.9 | +23:03:34 | 0.42±0.02 | 1.1± 0.2 | 1.5± 0.3 |
| DDO 210 | 0.9 | 0.16±0.01 | ... | 20:46:51.7 | -12:51:20 | 0.29±0.01 | 1.8± 0.1 | ... |
| DDO 216 | 1.1 | 0.52±0.01 | 1.77± 0.45 | 23:28:39.7 | +14:44:47 | 0.59±0.01 | 1.1± 0.0 | 0.3± 0.1 |
| F564-V3 | 8.7 | 0.63±0.09 | 0.73± 0.40 | 9:02:55.6 | +20:04:31 | 1.24±0.08 | 2.0± 0.3 | 1.7± 0.9 |
| IC 1613 | 0.7 | 0.53±0.02 | 0.71± 0.12 | 1:05:08.9 | +2:14:15 | 1.77±0.01 | 3.3± 0.1 | 2.5± 0.4 |
| LGS 3 | 0.7 | 0.16±0.01 | 0.27± 0.08 | 1:03:56.4 | +21:53:56 | 0.32±0.01 | 2.0± 0.1 | 1.2± 0.4 |
| M81dwA | 3.6 | 0.27±0.00 | 0.38± 0.03 | 8:23:52.5 | +71:01:31 | 0.71±0.03 | 2.6± 0.1 | 1.9± 0.2 |
| NGC 1569 | 3.4 | 0.46±0.02 | 0.85± 0.24 | 4:30:58.9 | +64:50:20 | 5.19±0.03 | 2.5± 0.1 | 1.3± 0.4 |
| NGC 2366 | 3.4 | 1.91±0.25 | 2.57± 0.80 | 7:29:36.2 | +69:16:22 | 6.79±0.03 | 3.6± 0.5 | 2.6± 0.8 |
| NGC 3738 | 4.9 | 0.77±0.01 | 1.16± 0.20 | 11:35:47.2 | +54:31:31 | 1.21±0.05 | 1.6± 0.1 | 1.0± 0.2 |
| NGC 4163 | 2.9 | 0.32±0.00 | 0.71± 0.48 | 12:12:09.2 | +36:10:27 | 0.47±0.03 | 1.5± 0.1 | 0.7± 0.4 |
| NGC 4214 | 3.0 | 0.75±0.01 | 0.83± 0.14 | 12:15:30.8 | +36:13:46 | 5.46±0.03 | 7.3± 0.1 | 6.6± 1.1 |
| NGC 6822 | 0.5 | 3.16±0.10 | 0.46±0.16 | 19:43:34.1 | -14:33:42 | 4.61±0.00 | 1.5± 0.1 | 10.0±3.5 |
| SagDIG | 1.1 | 0.32±0.05 | 0.57± 0.14 | 19:30:00.8 | -17:39:56 | 0.65±0.01 | 2.0± 0.3 | 1.1± 0.3 |
| WLM | 1.0 | 1.18±0.01 | 0.83± 0.16 | 0:01:46.9 | -15:27:52 | 2.06±0.01 | 1.7± 0.0 | 2.5± 0.5 |
| Haro 29 | 5.8 | 0.33±0.00 | 1.15± 0.26 | 12:26:18.3 | +48:29:46 | 0.86±0.06 | 2.6± 0.2 | 0.7± 0.2 |
| Haro 36 | 9.3 | 1.01±0.00 | 1.16± 0.13 | 12:46:59.4 | +51:36:53 | 1.79±0.09 | 1.8± 0.1 | 1.5± 0.2 |
| Mrk 178 | 3.9 | 0.19±0.00 | 0.38± 0.00 | 11:33:33.7 | +49:13:31 | 1.45±0.04 | 7.6± 0.2 | 3.8± 0.1 |
| VIIZw 403 | 4.4 | 0.53±0.02 | 1.02± 0.29 | 11:28:01.9 | +78:59:50 | 0.33±0.04 | 0.6± 0.1 | 0.3± 0.1 |

^a R_D is the disk scale length given by Herrmann et al. (2013).

^b R_{Br} is the radius at which the *V*-band surface brightness profile changes slope, as given by Herrmann et al. (2013).

^cRadius of the furthest *FUV* knot from the center of the galaxy determined in the plane of the galaxy. The galaxy disk geometry was determined from *V*-band images by Hunter & Elmegreen (2006). The uncertainty is assumed to be 2".

(2009), and compared our identifications of individual regions with theirs. The distance to the furthest knot from the center of the galaxy in the plane of the galaxy, R_{knot} , was determined by comparing the location of the knot to ellipses superposed that were used for surface photometry. The major axis and minor-to-major axis ratio of the ellipses were determined for the galaxy from the V -band image. We then identified the annulus or ellipse boundary at which the FUV knot fell. The R_{knot} are given in Table 1, along with the ratios of R_{knot} to the disk scale length, R_D , and to the break radius, R_{Br} . The break radius is the radius at which the exponential stellar surface brightness profile changes slope. Dwarf irregular galaxies, despite having irregular and sporadic star formation, have well-behaved exponential stellar disk profiles, even out to 6-10 R_D (Saha et al. 2010; Hunter et al. 2011; Bellazzini et al. 2014). These azimuthally-averaged profiles, like those in spirals, often show abrupt breaks, most often dropping in brightness into the outer disk more steeply than in the interior disk (Type II profiles) but occasionally dropping less steeply (Type III). Surface brightness profiles without breaks (Type I) are actually rare. R_D and R_{Br} were taken from Herrmann et al. (2013). Two galaxies (DDO 47, DDO 210) do not have breaks in their exponential disk surface brightness profiles.

The FUV regions are identified on the FUV images shown in Figure 1, along with the HI shown as contours from the integrated HI maps. The HI extends much further than the outermost FUV regions, which are usually located just inside the 5th or 6th contour, counting inwards from the outermost one. The HI column density there is $5 - 10 \times 10^{20}$ atoms cm^{-2} , which corresponds to $2.7 - 5.4 M_{\odot} \text{pc}^{-2}$ assuming a mean atomic weight of 1.36 times the Hydrogen mass. The HI maps are irregular, as expected for the dIrr morphology, and the FUV regions are often associated with one of these irregularities, indicating the presence of a local gas concentration. We show in §3.3 that the average HI density at the radius of the FUV region is several times less than this local density.

3. Analysis

3.1. Characteristics of the FUV regions

We have estimated ages and masses of the knots by fitting aperture photometry from the FUV , NUV , U , B , and V images (Hunter & Elmegreen 2006). We determined the brightness of the underlying stellar disk for subtraction from the region photometry for most of the regions using the mode of the counts in an annulus 5 pixels (1.35" to 5.67") wide and 2 pixels (0.54" to 4.6") in radius beyond the photometric aperture. Since the regions are generally in the far outer parts of the disk, they are not crowded and aperture photometry is adequate. For some galaxies, such as those in which the star formation is centrally con-

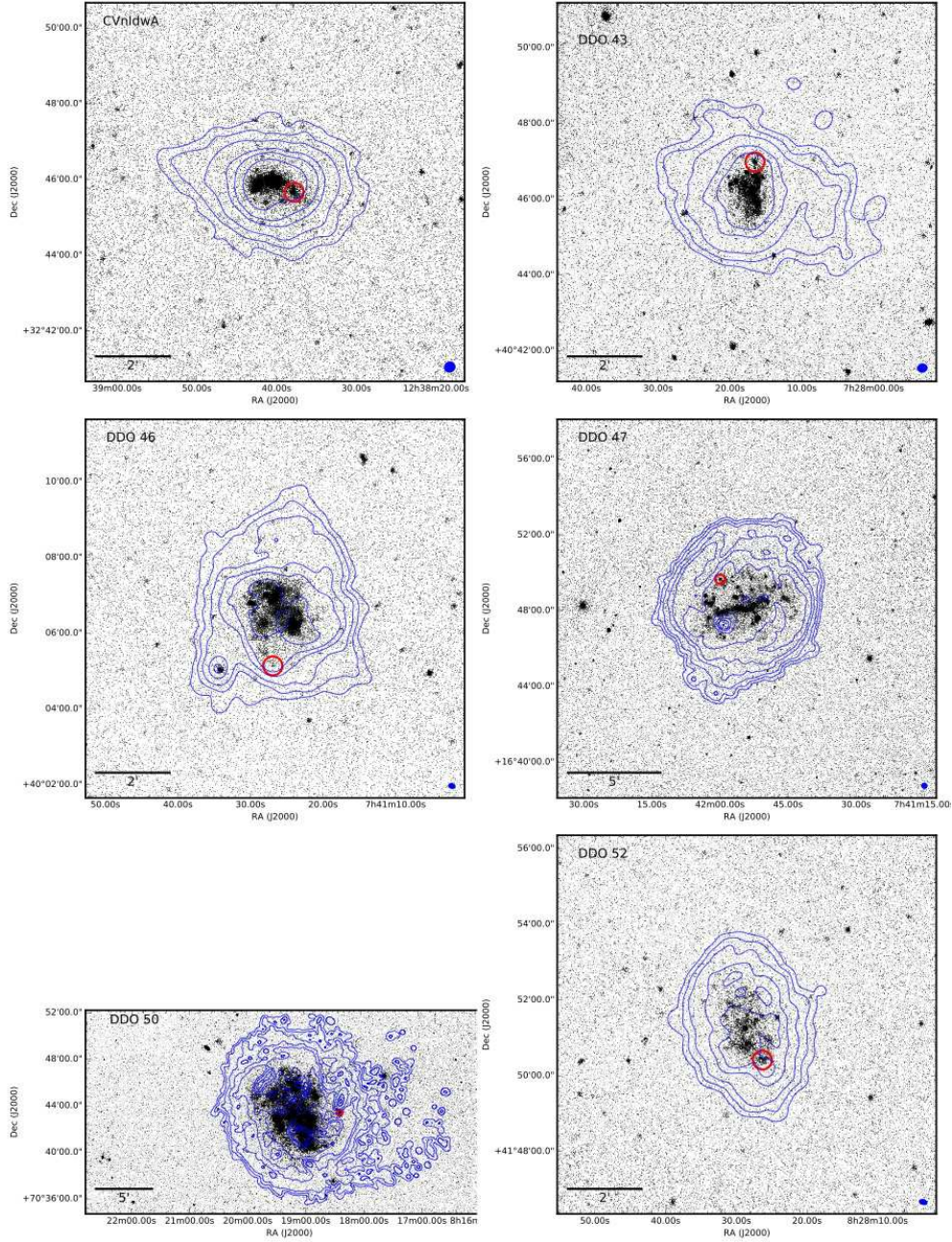


Fig. 1.— *FUV* images of the galaxies in our sample. The red circle outlines the distinct *FUV* region belonging to the galaxy that we considered to be at the furthest radius in the plane of the galaxy. The circle has a radius of $15''$ unless the aperture used for photometry of the region (given in Table 2) is larger; then the aperture radius is used. The blue contours are of the integrated natural-weighted HI map of the galaxy from Hunter et al. (2012) and outline column densities of 5, 30, 100, 300, 500, 1000, and 3000×10^{18} atoms cm^{-2} . The blue ellipse in the bottom right of each galaxy panel outlines the FWHM of the HI beam (major axis, minor axis, and position angle). (The complete figure set (7 pages) is available in the online journal).

centrated, the *FUV* regions are too crowded with other regions for an annulus around the region to give a reliable measure of underlying galaxy. For these galaxies (DDO 53, DDO 101, M81dwA, NGC 3738, NGC 4163, Haro 29, Haro 36, VII Zw 403), we determined the background from nearby areas at approximately the same disk surface brightness as that where the *FUV* region was found. No *UBV* photometry was available from our data for the *FUV* region in NGC 6822. The aperture radius, colors, and $E(B - V)$ used for reddening corrections are given in Table 2.

$E(B - V)$ includes foreground reddening from Burstein & Heiles (1984) and 0.05 mag for internal reddening. The internal reddening is half that determined from Balmer decrements in H II regions in a sample of 39 dIrr galaxies, as described in Hunter et al. (2010). The expectation is that these stars are not as embedded as one would find in H II regions. Furthermore, since most of these regions are in the outer disks of the dwarfs, extinction due to dust is expected to be minor. We use the reddening law of Cardelli et al. (1989) to produce the extinction in each optical filter. For the *GALEX* filters, we use $A_{FUV} = 8.24E(B - V)$ and $A_{NUV} = 7.39E(B - V)$ taken from Wyder et al. (2007) and discussed in relation to the LITTLE THINGS dwarfs by Hunter et al. (2010).

To model the ages and determine masses, we compared the integrated cluster photometry with cluster evolutionary models of Leitherer et al. (1999). These models trace the evolution of a $10^6 M_{\odot}$ cluster over time, assuming a Salpeter (1955) stellar initial mass function from 0.1 to $100 M_{\odot}$. We used the models for $Z = 0.004$ metallicity, since this is typical of the LITTLE THINGS dwarfs. See Billett et al. (2002) and Hunter et al. (2003) for more details on our color fitting procedure.

The ages and masses of the clusters are given in Table 2, values are shown as histograms in Figures 2 and 3, and mass is plotted against age in Figure 4. The uncertainties in the ages and masses represent the range of ages allowed by the colors. The ages are all less than 20 Myrs. Young ages are expected since the regions were selected to be bright knots of *FUV* emission. Masses range from $20 M_{\odot}$ to $1.3 \times 10^5 M_{\odot}$. There is no correlation between age or mass and distance from the center of the galaxy.

Eight of the galaxies in our sample were also analyzed by Melena et al. (2009). Working from the *NUV* images, they identified, not just the furthest regions, but all of the discrete regions in the galaxies. The ensembles of clusters of these 8 galaxies extended to radii that were comparable to ours: 0.7-1.1 times the radii where we identified our furthest *FUV* knots. Their ensembles included older clusters, but the masses of our regions are within the range of the masses found by Melena et al. (2009) out at their furthest radius. The exceptions are DDO 70 and DDO 210 which have masses that are lower by a factor of 15 and 20, respectively, in our study. Thus, we conclude that the regions we identified in our study are

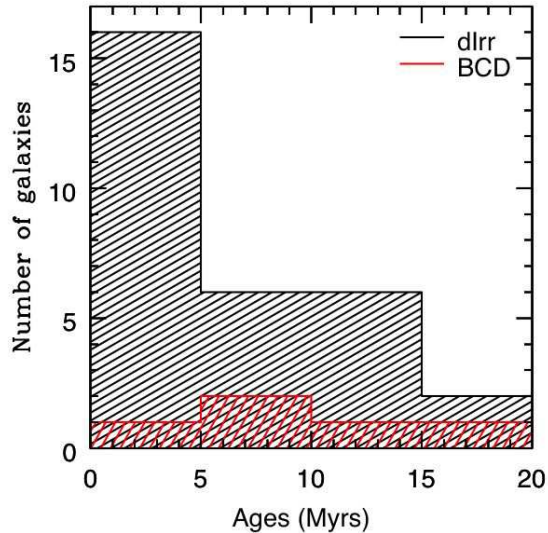


Fig. 2.— Histogram of the ages of the furthest FUV knots found by fitting $FUV - NUV$, $U - B$, and $B - V$ colors with Starburst99 cluster evolutionary models (Leitherer et al. 1999).

not unusual compared to the collection of star clusters one finds in the outer disks of dIrr galaxies in general.

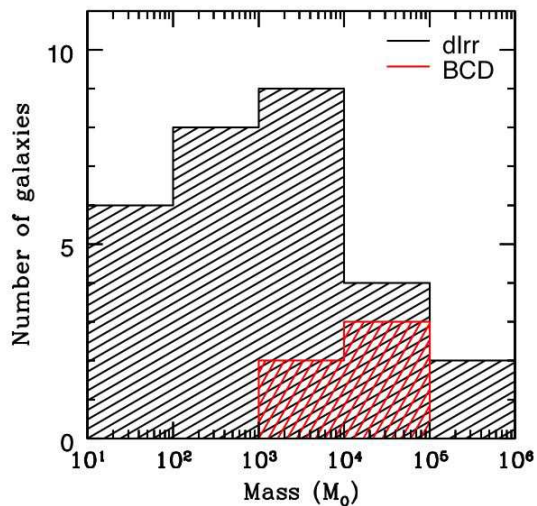


Fig. 3.— Histogram of the masses of the furthest FUV knots, determined from the age and M_V using Starburst99 cluster evolutionary models (Leitherer et al. 1999).

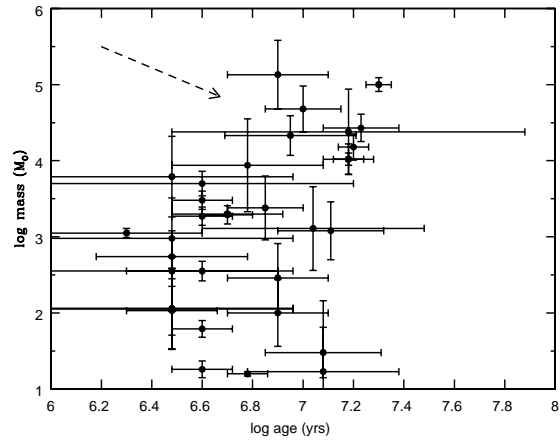


Fig. 4.— Mass versus age of the *FUV* knots. The uncertainties in the ages and masses represent the range of ages allowed by the colors. The dashed vector denotes the consequences of adding a reddening of $E(B - V)=0.1$.

Table 2. Photometry^a, ages and masses of *FUV* regions

| Galaxy | E(B-V) | r(arcs) ^b | m_{FUV} | $M_{FUV,0}$ | $(FUV - NUV)_0$ | $M_{V,0}$ | $(B - V)_0$ | $(U - B)_0$ | Nfit ^c | Age (Myrs) ^d | Mass (M_{\odot}) |
|----------|--------|----------------------|-----------|---------------|-----------------|---------------|--------------|--------------|-------------------|-------------------------|----------------------|
| CVnIdwA | 0.055 | 5.7 | 20.786 | -6.995±0.068 | -0.251±0.078 | -6.982±0.071 | -0.001±0.089 | -0.627±0.142 | 3 | 3± 2 | 360± 250 |
| DDO 43 | 0.105 | 5.7 | 21.009 | -8.452±0.080 | -0.141±0.101 | -8.771±0.122 | -0.355±0.138 | -0.802±0.074 | 3 | 5± 1 | 2000± 490 |
| DDO 46 | 0.103 | 5.7 | 23.051 | -5.876±0.229 | -1.178±0.611 | -5.221±0.832 | -1.063±0.885 | -1.730±0.271 | 0 | ... | ... |
| DDO 47 | 0.073 | 7.9 | 20.711 | -7.869±0.063 | -0.383±0.091 | -8.045±0.122 | -0.123±0.147 | -0.663±0.100 | 3 | 3± 2 | 960± 670 |
| DDO 50 | 0.073 | 14.7 | 18.804 | -8.854±0.008 | -0.123±0.010 | -8.475±0.061 | -0.203±0.068 | -1.078±0.049 | 3 | 4± 1 | 1900± 440 |
| DDO 52 | 0.080 | 7.9 | 20.977 | -9.087±0.082 | -0.422±0.118 | -9.547±0.104 | 0.119±0.133 | -0.608±0.128 | 3 | 4± 3 | 5000± 1500 |
| DDO 53 | 0.075 | 5.0 | 19.402 | -8.380±0.015 | -0.193±0.018 | -8.787±0.003 | 0.022±0.004 | -0.914±0.004 | 3 | 5± 2 | 2000± 90 |
| DDO 63 | 0.062 | 34.0 | 19.212 | -8.743±0.013 | 0.065±0.016 | -9.853±0.082 | 0.007±0.096 | -0.042±0.138 | 2 | 16± 2 | 15000± 4700 |
| DDO 69 | 0.050 | 9.1 | 21.245 | -3.270±0.105 | -0.055±0.138 | -3.362±0.116 | 0.099±0.131 | -0.766±0.130 | 3 | 12± 5 | 30± 16 |
| DDO 70 | 0.063 | 5.7 | 21.486 | -4.084±0.127 | -0.332±0.176 | -3.466±0.299 | -0.213±0.351 | -1.008±0.185 | 3 | 4± 1 | 18± 4 |
| DDO 75 | 0.068 | 4.7 | 20.101 | -5.469±0.050 | -0.315±0.062 | -5.664±0.049 | 0.320±0.067 | -1.113±0.063 | 2 | 3± 1 | 110± 55 |
| DDO 87 | 0.050 | 6.8 | 21.938 | -7.495±0.152 | -0.793±0.256 | -7.439±0.184 | 0.514±0.262 | -0.744±0.312 | 1 | 3± 3 | 550± 16 |
| DDO 101 | 0.058 | 6.8 | 20.447 | -8.584±0.059 | 0.043±0.070 | -9.519±0.006 | 0.308±0.010 | -0.806±0.013 | 1 | 15± 3 | 10600± 3900 |
| DDO 126 | 0.050 | 13.6 | 20.077 | -8.374±0.054 | -0.169±0.070 | -9.000±0.053 | 0.191±0.073 | -0.695±0.077 | 2 | 7± 2 | 2400± 1500 |
| DDO 133 | 0.053 | 11.3 | 18.827 | -8.893±0.011 | -0.184±0.013 | -8.992±0.020 | 0.159±0.025 | -1.002±0.023 | 2 | 4± 1 | 3000± 710 |
| DDO 154 | 0.058 | 10.2 | 20.747 | -7.094±0.087 | -0.858±0.153 | -5.594±0.524 | -0.828±0.565 | 0.440±0.713 | 0 | ... | ... ¹⁰ |
| DDO 167 | 0.050 | 4.5 | 21.541 | -6.576±0.104 | 0.018±0.115 | -7.320±0.096 | 0.394±0.116 | -0.626±0.099 | 2 | 13± 5 | 1200± 710 |
| DDO 168 | 0.050 | 6.8 | 19.342 | -8.825±0.036 | 0.176±0.038 | -11.396±0.008 | 0.507±0.015 | 0.725±0.037 | 1 | 20± 2 | 100300±19000 |
| DDO 187 | 0.050 | 5.7 | 20.289 | -6.423±0.050 | -0.232±0.054 | -6.667±0.078 | 0.000±0.097 | -0.568±0.071 | 3 | 4± 2 | 350± 90 |
| DDO 210 | 0.085 | 5.4 | 21.306 | -3.465±0.098 | -0.616±0.148 | -3.694±0.146 | -0.225±0.175 | -0.507±0.111 | 3 | 6± 1 | 16± 1 |
| DDO 216 | 0.073 | 5.0 | 21.297 | -3.910±0.095 | -0.122±0.108 | -5.238±0.037 | 0.404±0.046 | -0.651±0.032 | 2 | 8± 3 | 100± 60 |
| F564-V3 | 0.068 | 4.9 | 22.388 | -7.310±0.172 | -0.450±0.262 | -7.767±0.213 | 0.080±0.249 | 0.028±0.249 | 2 | 2± 2 | 1100± 150 |
| IC 1613 | 0.055 | 23.2 | 18.606 | -5.619±0.027 | -0.295±0.038 | -5.718±0.111 | -0.006±0.121 | -0.565±0.096 | 3 | 3± 2 | 110± 80 |
| LGS3 | 0.085 | 5.7 | 23.321 | -0.905±0.395 | 0.020±0.518 | -2.787±0.118 | 0.459±0.162 | -0.077±0.160 | 1 | 12±12 | 20± 15 |
| M81dwA | 0.072 | 6.8 | 21.248 | -6.534±0.026 | -0.049±0.033 | -11.477±0.002 | 0.927±0.004 | 0.675±0.010 | 1 | 10± 3 | 48000±24000 |
| NGC 1569 | 0.558 | 4.2 | 22.336 | -5.321±0.095 | 0.033±0.115 | -10.418±0.025 | 0.161±0.033 | -1.260±0.024 | 3 | 15±12 | 24000±18000 |
| NGC 2366 | 0.093 | 33.6 | 19.557 | -8.101±0.051 | -0.149±0.070 | -10.489±0.020 | 0.590±0.025 | -0.135±0.023 | 1 | 6± 3 | 8800± 6700 |
| NGC 3738 | 0.050 | 4.5 | 16.175 | -12.276±0.008 | -0.099±0.009 | -13.063±0.001 | 0.161±0.002 | -0.706±0.002 | 2 | 8± 3 | 130000±87000 |
| NGC 4163 | 0.050 | 4.5 | 18.736 | -8.576±0.010 | 0.050±0.012 | -9.520±0.002 | 0.324±0.004 | -0.579±0.009 | 2 | 15± 2 | 11000± 1800 |
| NGC 4214 | 0.050 | 6.3 | 21.373 | -6.012±0.089 | -0.348±0.118 | -5.738±0.146 | -0.230±0.157 | -0.770±0.071 | 3 | 3± 2 | 110± 80 |
| NGC 6822 | 0.265 | 120.0 | 16.710 | -6.785±0.016 | -0.239±0.021 | ... | ... | ... | 1 | 3± 1 | ... |
| SagDIG | 0.188 | 4.9 | 20.694 | -4.513±0.083 | -0.117±0.104 | -6.390±0.019 | -0.103±0.022 | -0.793±0.022 | 3 | 8± 3 | 290± 180 |
| WLM | 0.068 | 6.8 | 19.524 | -5.476±0.041 | -0.275±0.051 | -4.796±0.071 | -0.078±0.080 | -0.909±0.047 | 3 | 4± 1 | 60± 14 |

Table 2—Continued

| Galaxy | E(B-V) | r(arcs) ^b | m_{FUV} | $M_{FUV,0}$ | $(FUV - NUV)_0$ | $M_{V,0}$ | $(B - V)_0$ | $(U - B)_0$ | Nfit ^c | Age (Myrs) ^d | Mass (M_{\odot}) |
|------------|--------|----------------------|-----------|---------------|-----------------|---------------|--------------|--------------|-------------------|-------------------------|----------------------|
| Haro 29 | 0.050 | 4.9 | 19.518 | -9.299±0.038 | 0.025±0.043 | -10.358±0.002 | 0.118±0.003 | -0.562±0.004 | 3 | 17± 5 | 27000± 9000 |
| Haro 36 | 0.050 | 4.9 | 19.777 | -10.065±0.042 | -0.079±0.050 | -10.833±0.003 | 0.179±0.005 | -0.857±0.008 | 2 | 9± 4 | 21000± 9400 |
| Mrk 178 | 0.050 | 6.7 | 20.271 | -7.684±0.056 | 0.159±0.064 | -7.478±0.049 | -0.260±0.051 | -0.992±0.029 | 2 | 11± 7 | 1300± 900 |
| VII Zw 403 | 0.073 | 4.3 | 18.209 | -10.008±0.021 | -0.309±0.025 | -10.066±0.002 | -0.049±0.003 | -0.808±0.003 | 3 | 3± 2 | 6100± 4300 |

^a FUV magnitudes are AB magnitudes. The UBV magnitudes are on the standard Landolt (1992) system.

^bRadius of photometry aperture in arcseconds.

^cNumber of colors ($FUV - NUV$, $B - V$, $U - B$) used in the age determination. An Nfit of 1 means the $FUV - NUV$ color was used, a value of 2 means either $U - B$ or $B - V$ was also used, and a value of 3 means a consistent age was determined for all three colors.

^dUncertainties represent the range of ages allowed by the colors. Derivations of ages consistent with the observed colors were not possible for LGS3, WLM, and NGC 6822.

3.2. Locations of the *FUV* regions

Histograms of the ratios R_{knot}/R_D and R_{knot}/R_{Br} are shown in Figure 5. There is structure due to star formation present in almost all of the outer disks. All of the furthest *FUV* knots in the dIrr galaxies are beyond one disk scale length and 69% are beyond $2R_D$. A few (DDO 70 and NGC 4214) are out as far as $7-8R_D$. In terms of the break in the *V*-band surface brightness profiles, in 57% of the dIrr galaxies the furthest *FUV* knots are at radii $\leq 2R_{Br}$, and so the regions are found roughly near the break. In two of the galaxies (DDO 75 and NGC 6822) the regions are found around $10R_{Br}$.

NGC 6822 is one of the extreme dIrr galaxies with a R_{knot}/R_{Br} ratio of 10. The *FUV* region is located in an HI cloud to the northwest of the galaxy center at a distance of 4.6 kpc. This region had been suggested to be a companion that is interacting with NGC 6822 (de Blok & Walter 2000; Komiyama et al. 2003), but an *HST* study of the stellar populations of this region and others along the HI extent found that the star formation histories of all six of their positions are similar over the past 500 Myr (Cannon et al. 2012). Cannon et al. (2012) argue that the “companion” has an old stellar population that is like that of the extended halo of NGC 6822. Therefore, we include it here as the furthest *FUV* region in NGC 6822.

DDO 75 is also a dIrr with a R_{knot}/R_{Br} ratio of 10, but it also has a peculiar surface brightness profile. The *V*-band surface brightness profile is flat to mildly increasing in brightness from the center to 0.7 kpc, and then the surface brightness drops like a normal exponential profile to a radius of 1.3 kpc (Herrmann et al. 2013). After that, as the surface brightness becomes fainter with radius, there are superposed up and down wiggles in the surface brightness profile (Bellazzini et al. 2014). Therefore, R_D may not be as well defined as it is in other galaxies.

The two dIrrs with the highest R_{knot}/R_D ratios are DDO 70 and NGC 4214. The surface brightness profile of DDO 70 is also flat but only to a radius of 0.1 kpc and then is well-behaved after that (Bellazzini et al. 2014). NGC 4214 has a steeper profile in the inner disk, to a radius of 0.8 kpc. Beyond that radius, the surface brightness drops as a normal exponential. In spite of these small peculiarities, it is not obvious what is special about DDO 70 and NGC 4214 that they would have *FUV* knots at such large R_D ; there are other dwarfs that are more peculiar than these with smaller R_{knot}/R_D .

For the BCDs, 43% of the furthest *FUV* regions are beyond $2R_D$ and 80% are found relatively near the break radius, with only one further out at $3-4R_{Br}$. Statistics are poor, of course, with only five BCDs. Nevertheless, we expect BCDs to be more centrally concentrated than normal dIrrs, and their R_{knot} are roughly in agreement with that. The BCDs in

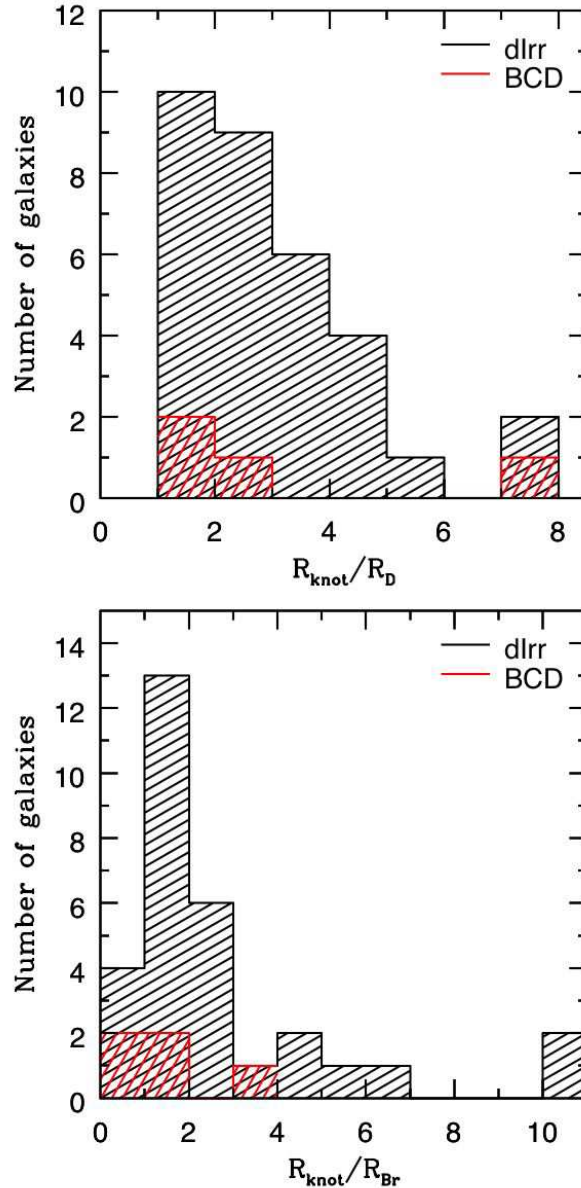


Fig. 5.— Histogram of the distance to the furthest knot of FUV emission for each galaxy relative to the disk scale length R_D and the break radius R_{Br} . The break radius is the radius at which the stellar exponential profile changes slope. Two dIrr galaxies in our sample do not have breaks.

the LITTLE THINGS sample have also been shown to likely be the result of an interaction or merger that has driven material towards the central regions of the galaxies (Ashley et al. 2013, 2014).

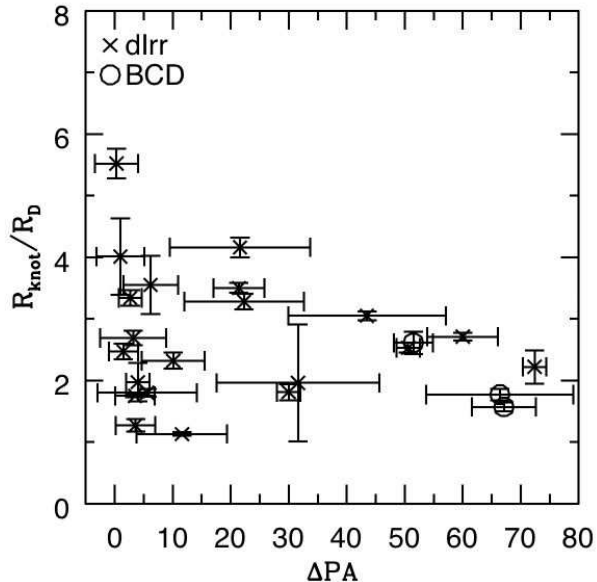


Fig. 6.— R_{knot}/R_D plotted versus ΔPA , the difference between the position angle of the major axis of the stellar disk, determined from V -band images, and the position angle of the H I kinematics, determined from fits to the bulk velocity field of the gas (Oh et al. 2015). We assume an uncertainty in the optically derived PA of 2° and the uncertainty in the H I kinematics is from Oh et al. (2015).

3.3. Relationships of FUV regions to other galactic characteristics

To explore a potential connection between large-scale structural peculiarities and the extended nature of star formation in dwarfs, we look at the relationship between R_{knot}/R_D and differences between optical and H I kinematic position angles. The position angle of the optical major axis was determined from smoothed outer isophotes of the V -band images (Hunter & Elmegreen 2006), and the H I kinematic major axis was determined from iterative fits to the bulk velocity field of the gas (Oh et al. 2015). Twenty-six of the LITTLE THINGS galaxies were in the study by Oh et al. (2015) and all but two are included in this study. We would expect these two position angles - one describing the stellar disk and one describing the gas disk - to be co-located, but over half of the LITTLE THINGS galaxies have ΔPA that are larger than 20° . The large differences could represent some peculiarity of the galaxy structure. In Figure 6 we plot R_{knot}/R_D as a function of the difference in the position angles. We find that galaxies with large ΔPA are not distinguished in terms of R_{knot}/R_D compared to those with small ΔPA , although there is a decline in the upper envelope such that R_{knot}/R_D declines as ΔPA increases.

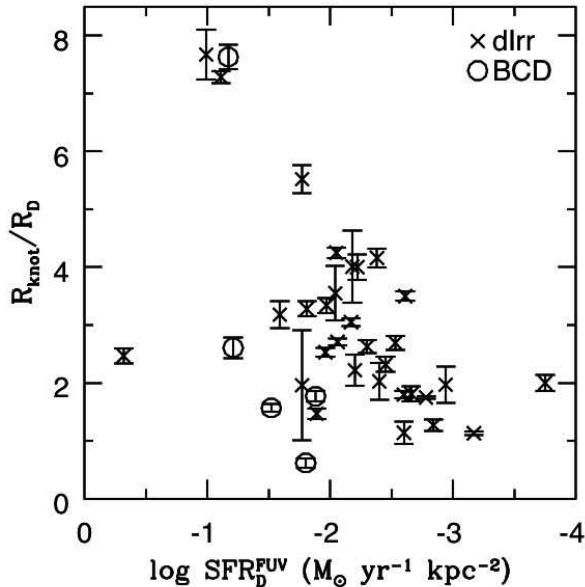


Fig. 7.— R_{knot}/R_D plotted versus the log of the star formation rate determined from the integrated FUV luminosity (Hunter et al. 2010; Zhang et al. 2012). The SFR is normalized to the area of the galaxy within one disk scale length: πR_D^2 . The uncertainties in the SFR_D^{FUV} are smaller than the point size and are not plotted.

In Figure 7 we plot R_{knot}/R_D as a function of the galactic integrated SFR determined from the FUV luminosity (Hunter et al. 2010; Zhang et al. 2012): $\log SFR_D^{FUV}$ ($M_\odot \text{yr}^{-1} \text{kpc}^{-2}$). The SFR is normalized to the area contained within one disk scale length. The thought here is that if a galaxy has a higher SFR, it might also have more extended star formation. In Figure 7 we see that, with one exception, the galaxies with the highest SFRs do also have the furthest FUV knots in terms of disk scale lengths. In addition, the galaxies with lowest SFRs have among the lower R_{knot}/R_D ratios. However, the galaxies in between these extremes display a range of SFRs and a range of R_{knot}/R_D without a clear trend.

To explore the relationship between the extent of the FUV knots and the average gas densities at that radius, we plot R_{knot}/R_D against the log of the azimuthally-averaged HI surface density Σ_{HI} (Hunter et al. 2012) at the radius of R_{knot} in Figure 8. There is no trend of R_{knot}/R_D with Σ_{HI} , but most points are centered around a value of $1 M_\odot \text{pc}^{-2}$.

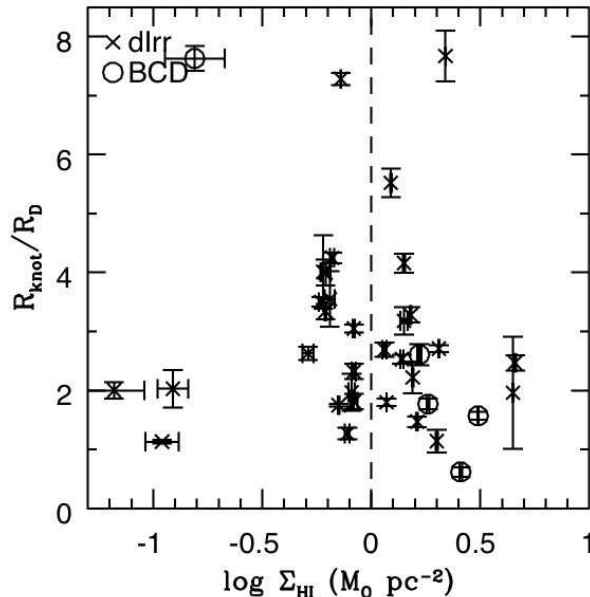


Fig. 8.— R_{knot}/R_D plotted versus the log of the azimuthally-averaged H I surface density (Hunter et al. 2012) at the radius of R_{knot} . The uncertainties in Σ_{HI} are determined from the rms in the integrated H I map and the number of beams within the annulus over which an average was taken. The rms in the integrated H I map was determined from the uncertainty in individual channels and an assumed average number of channels contributing to each pixel (see de Blok et al. 2008).

4. Environment for star formation near the knots

Fifteen galaxies in the present study have outer star formation knots within the radial range of the survey of dlrr in Elmegreen & Hunter (2015), for which we determined gas column densities, scale heights, midplane densities, and Toomre Q values as a function of radius for gas and stars. The scale heights and densities came from solutions to the vertical equilibrium of a three component fluid consisting of gas, stars, and dark matter, using observed velocity dispersions and column densities. The Q values also included the observed rotation curves to give the epicyclic frequency. Figures 9 and 10 show histograms of these quantities for gas and stars, respectively, at the radii of the FUV knots. Comparing the two figures, the average densities and column densities for the stars are much lower than for the gas at these radii, emphasizing that the FUV knots are in gas-dominated regions. Q is high for both gas and stars, but higher for stars because of the lower stellar surface densities. The scale heights at these radii are about the same for the two components.

The average environment at the radius of an FUV region is important for understanding

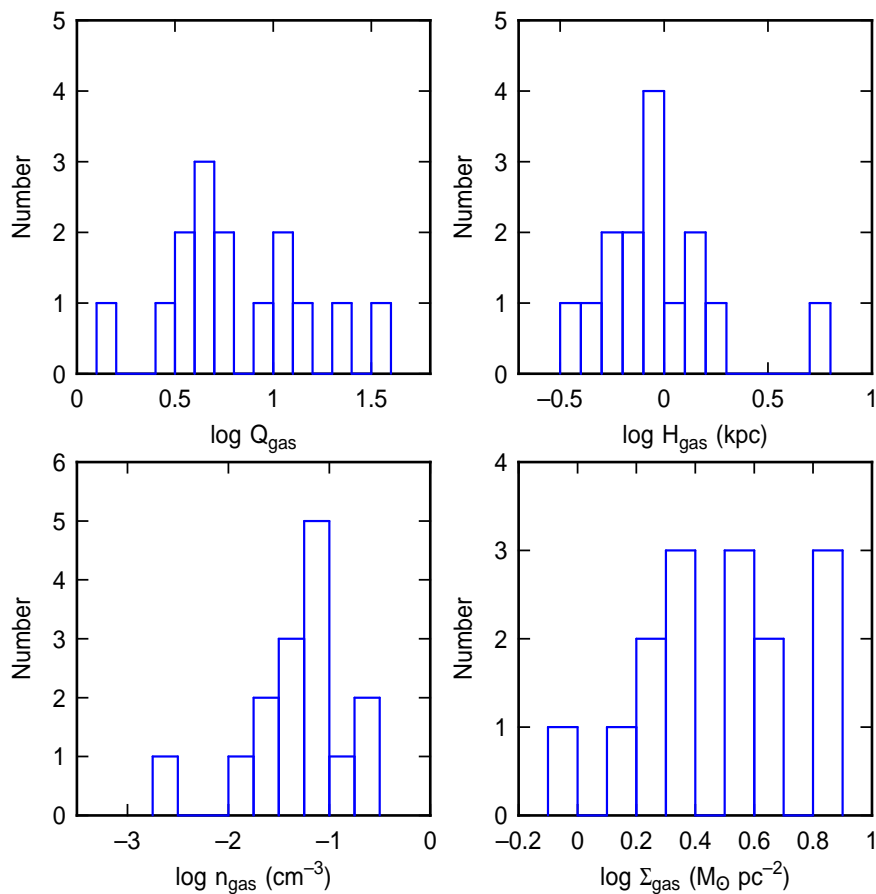


Fig. 9.— Distribution of environmental parameters for 15 *FUV* knots in the present study that have measurements in the same galaxy and radial range considered in Elmegreen & Hunter (2015). The parameters are all for the gas: Toomre Q , scale height H_{gas} , midplane density n_{gas} , and surface density including He and heavy elements.

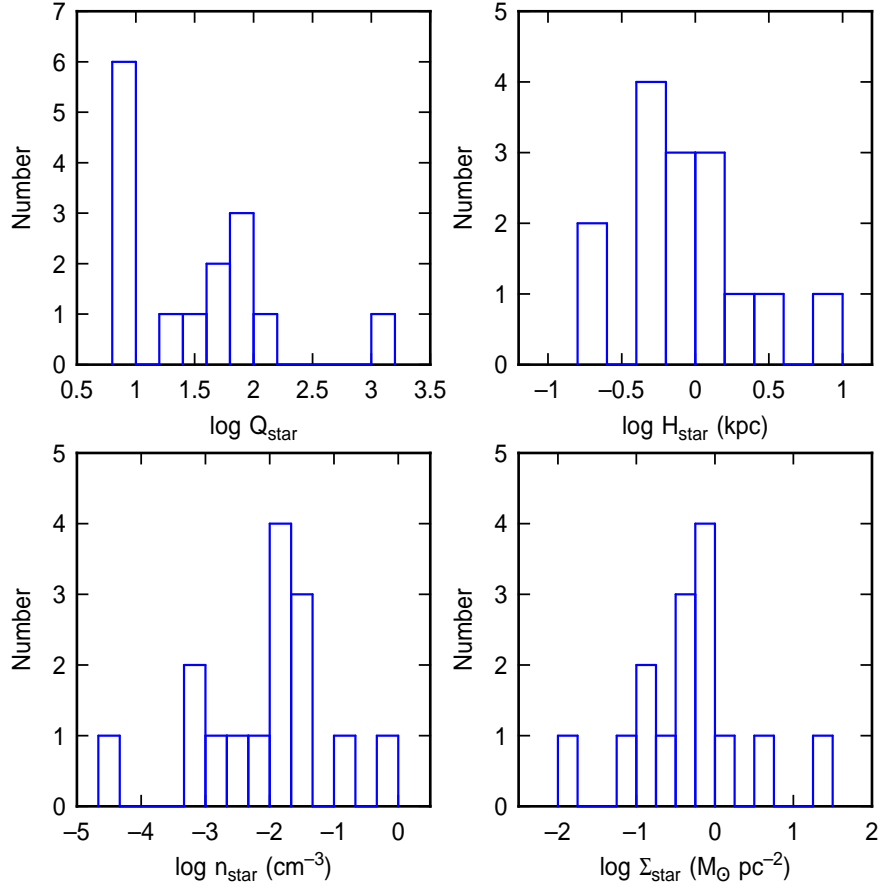


Fig. 10.— Distribution of environmental parameters as in Figure 9 but for stars at the radius of the *FUV* knots.

how the gas first got concentrated into a cloud to begin the process of star formation. HI excesses near the identified regions are sometimes directly evident as deformations in the HI contours in Figure 1. Almost all of the *FUV* knots occur in larger-scale *FUV* structures too. These large-scale structures typically have a size comparable to the disk scale length. Their formation would presumably involve processes that operate on the local average dynamical time, which depends on the average midplane density. In these far-outer regions, the average midplane density is typically 10 or more times lower than the gas density in the solar neighborhood (which is about 1 cm^{-3}) as a result of both the low HI surface density and the large gas scale height from weak gravity (Fig. 9). Consequently, the dynamical time over the region that the star-forming gas came from was long: $t_{\text{ff}} = 140 \text{ Myr}$ for midplane gas density n_{gas} at the typical value of 0.1 cm^{-3} . The free fall time is taken to be $t_{\text{ff}} = (3\pi/32G\rho)^{1/2}$ for $\rho = 1.36n_{\text{gas}}m_{\text{H}}$ and $m_{\text{H}} = 1.67 \times 10^{-24} \text{ g}$. This time is 20 times the average age of the knots, which is 7 Myr from Table 2. Unless there is a relatively dense layer of undetected molecular gas near the midplane or some triggering event like an extragalactic cloud impact, the formation of the observed knots by large-scale dynamical processes requires a relatively long time. This suggests there was a threshold density or column density for the cluster to form so the cloud could grow without early disruption from the first few stars.

A threshold surface density for star formation in the outer parts of dIrr galaxies is most likely not the same as that in the solar neighborhood (e.g., Lada et al. 2010) because the pressures and metallicities in dIrrs are much lower. The threshold column density for strong self-gravity in a cloud scales as the square root of the boundary pressure, with collapse proceeding exponentially slower as $P/(G\Sigma_{\text{gas}}^2)$ increases (Padoan et al. 2012). With P lower by a factor of 10, the threshold column density for strong gravity in our case should be lower by a factor of about 3. That would make it $\Sigma_{\text{thresh}} \sim 40 M_{\odot} \text{ pc}^{-2}$ inside the star-forming region of a cloud, if we take the solar neighborhood threshold as $116 M_{\odot} \text{ pc}^{-2}$ from Lada et al. (2010). Another threshold involves opacity and the formation of strong coolants, like CO. The opacity threshold, measured in terms of a mass column density threshold, scales inversely with metallicity, and the metallicities for these dIrrs are lower than solar by a factor of about 8. Thus the mass column density for an opacity threshold should be 8 times larger in these dIrrs than in the solar neighborhood. If $\sim 1.5 \text{ mag}$ is the local threshold for CO formation (Glover & Clark 2012), then the corresponding surface density of gas would be $230 M_{\odot} \text{ pc}^{-2}$ for the clouds that formed our *FUV* knots. This is what we observe for CO emission in the dIrr WLM, where the metallicity has this value (Rubio et al. 2015). If both strong self-gravity and high extinction are required for star formation, then the larger of these two thresholds should apply. However, if strong self-gravity alone is required and the opacity threshold automatically follows during the ensuing collapse, then only the lower

threshold is required. This cloud threshold, $\sim 40 M_{\odot} \text{ pc}^{-2}$, is a factor of ~ 13 larger than the average surface density of HI at the radius of the *FUV* knots, which is $\sim 3 M_{\odot} \text{ pc}^{-2}$ from Figures 8 and 9. A factor of 13 increase in column density corresponds to a factor of $13^{1/2} \sim 3.6$ contraction in two dimensions. This is about the same factor that clouds in the solar neighborhood would have to contract if the cloud threshold for star formation always scales with the square root of the ambient pressure. In this sense, star formation in outer dIrr disks may not be qualitatively different from other star formation.

This picture of star formation at the local dynamical rate changes if a particular event was triggered by something rapid, such as an extragalactic cloud impact. Some BCDs and extremely low-metallicity dwarf galaxies have single dominant star-forming regions with lower metallicities than in the rest of the galaxy (Sánchez Almeida et al. 2013, 2014, 2015). These regions could be the sites of extragalactic cloud impacts with low metallicities from nearly pristine gas. One example, Kiso 5639 (Elmegreen et al. 2016), has a star formation rate surface density in a $\sim 800 \text{ pc}$ region that is $\sim 5\times$ larger than the value expected from the Kennicutt-Schmidt relation at the likely gas surface density. The total young mass there is $\sim 10^6 M_{\odot}$ for a $\sim 10^8 M_{\odot}$ galaxy. These regions are all much larger and brighter than the *FUV* regions studied here, which look more typical for disk galaxies, although they formed at extremely low gas densities.

5. Does star formation occur in the far-outer regions?

One of the motivations for the present study was to determine if star formation could account for the outer *FUV* disks of dIrr galaxies, as opposed to stellar scattering from the inner disk. Here we compare the star formation rate inside each *FUV* knot, obtained from the ratio of the knot mass to the age, to the total rate inside an annulus of width R_D at the radius of the knot, as determined from the average Kennicutt-Schmidt (KS) relation for dIrrs at the local gas surface density (Elmegreen & Hunter 2015). If the total rate in the small knot is comparable to the total rate expected from the gas in the annulus, which is based on large-scale averages from many other observations, then one might conclude that star-forming regions like these can generally populate outer disks. If the annular rate is much larger than the local rate, then either we are missing *FUV* regions that are too small, faint, or dispersed to detect (e.g., Pellerin et al. 2008), or the average KS relation over-estimates the star formation rate at and below a gas surface density of $\sim 1 M_{\odot} \text{ pc}^{-2}$, where our *FUV* regions begin to disappear.

Such an over-estimate would imply that star formation virtually stops below $\sim 1 M_{\odot} \text{ pc}^{-2}$, according to our understanding of conventional processes (e.g., Kennicutt & Evans

2012). In that case, stellar scattering from the inner disk would seem to be important in filling the outer disk with stars. The outer disks have relatively smooth exponential radial profiles in V -band down to $\sim 0.1 M_\odot \text{ pc}^{-1}$ or lower (Herrmann et al. 2013). This is below the average stellar surface density at the radius of the FUV regions, as shown in Figure 10.

The left-hand panel of Figure 11 shows a histogram of star formation rates in the FUV knots. There is a wide range of rates, primarily because the regions vary a lot in mass and age. The middle panel shows a histogram of the ratio of the theoretical star formation rate in an annulus of width R_D around a knot to the rate in the knot. The right-hand panel shows the ratio of the theoretical rate integrated from the knot radius to infinity compared to the knot rate. For the theory, we use the expression

$$\Sigma_{\text{SFR}} = 1.7 \times 10^{-5} \Sigma_{\text{gas}}^2 M_\odot \text{ Myr}^{-1} \text{ pc}^{-2} \quad (1)$$

for H I surface density Σ_{gas} in $M_\odot \text{ pc}^{-2}$. This implies that in the annulus,

$$SFR = 2\pi R_{\text{knot}} R_D \Sigma_{\text{SFR}} M_\odot \text{ Myr}^{-1} \quad (2)$$

and for the integral

$$SFR = 2\pi R_D (R_D + R_{\text{knot}}) \Sigma_{\text{SFR}} M_\odot \text{ Myr}^{-1}. \quad (3)$$

The theoretical rate follows from the expression $\Sigma_{\text{SFR}} = \epsilon_{\text{ff}} \Sigma_{\text{gas}} / t_{\text{ff}}$ for a pure gas disk after substituting $\rho = \Sigma_{\text{gas}} / (2H)$ and $H = \sigma^2 / (\pi G \Sigma_{\text{gas}})$ inside the equation for free fall time given in the previous section, i.e.,

$$1/t_{\text{ff}} = 4G \Sigma_{\text{gas}} / [3^{1/2} \sigma]. \quad (4)$$

The theoretical rate compares well with observations of 20 dIrr galaxies if $\epsilon_{\text{ff}} = 0.01$ and the velocity dispersion is the observed value of $\sigma \sim 6 \text{ km s}^{-1}$ (Elmegreen & Hunter 2015; Elmegreen 2015). It also agrees with observations in the outer parts of spiral galaxies, which are gas-dominated like the dIrrs (Elmegreen 2015). This is the steep part of the KS relation, beyond the main disks of spirals, where atoms dominate molecules, gas dominates stars, and the total consumption time approaches 100 Gyrs (Bigiel et al. 2008, 2010). Note that equation (4) gives $t_{\text{ff}} = 590 \text{ Myr}$ for $\Sigma_{\text{gas}} = 1 M_\odot \text{ pc}^{-2}$ and $\sigma = 6 \text{ km s}^{-1}$, so the gas consumption time would be $t_{\text{ff}}/\epsilon = 59 \text{ Gyr}$ with $\epsilon = 0.01$. For equation (3), we assume that the gas disk has an exponential radial profile with a scale length twice that of the V -band disk, as found for the 20 dIrrs and for the outer parts of 23 blue spirals by Wang et al. (2014).

The middle and right-hand panels in Figure 11 suggest that the annuli around the knots and the outer disks would have $\sim 8\times$ larger star formation rates than the knots have now, given the KS relation for average rates extrapolated to the local average gas surface densities around the knots. Figure 12 illustrates this point by plotting the two theoretical

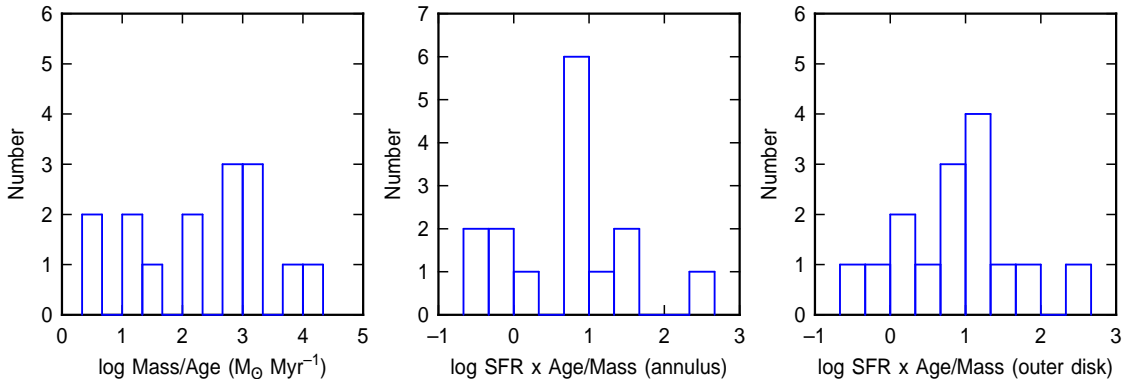


Fig. 11.— (left) The distribution of the ratio of mass divided by age for the *FUV* knots, as an approximation to the average star formation rate. (middle) The ratio of the total theoretical star formation rate in an annulus of width R_D centered on the knot to the average rate in the knot. (right) The ratio of the total theoretical star formation rate at all radii equal to and larger than the radius of the knot to the average rate in the knot. The theoretical rate comes from the Kennicutt-Schmidt relation in equation 1 assuming an exponential gas disk with a scale length that is twice R_D .

star formation rates for each knot location versus the knot’s star formation rate. Red dots are for the annulus and blue dots are for the outer disk. For the largest knots the two rates agree well, but for the smallest knots, the star formation rates fall short of the outer-disk expectations by a factor of ~ 10 . As mentioned above, this shortfall could be because smaller, fainter and more dispersed regions cannot be seen in our data, or because the SFR is actually below the extrapolated KS relation at $\sim 1 M_\odot \text{ pc}^{-2}$.

6. Summary

We have identified on *GALEX* images the furthest out distinct *FUV* knot in the LITTLE THINGS sample of dIrr and BCD galaxies that we are confident belong to the galaxy. These knots are found at distances from the center of the galaxies of 1 to 8 disk scale lengths and have ages of ≤ 20 Myrs and masses of $20 M_\odot$ to $1 \times 10^5 M_\odot$. The presence of young clusters in the outer disks of dwarf galaxies shows that dIrrs do have *in situ* star formation taking place in their outer disks. Most regions are found around an HI surface density of $1 M_\odot \text{ pc}^{-2}$, making this look like a threshold for the formation of prominent OB associations.

The environments of these remote star-forming regions are extreme compared to the solar neighborhood and inner Milky Way (§4), or even compared to the inner parts of dIrr galaxies. The average pressures and midplane densities are lower by a factor of ~ 10 , the disks

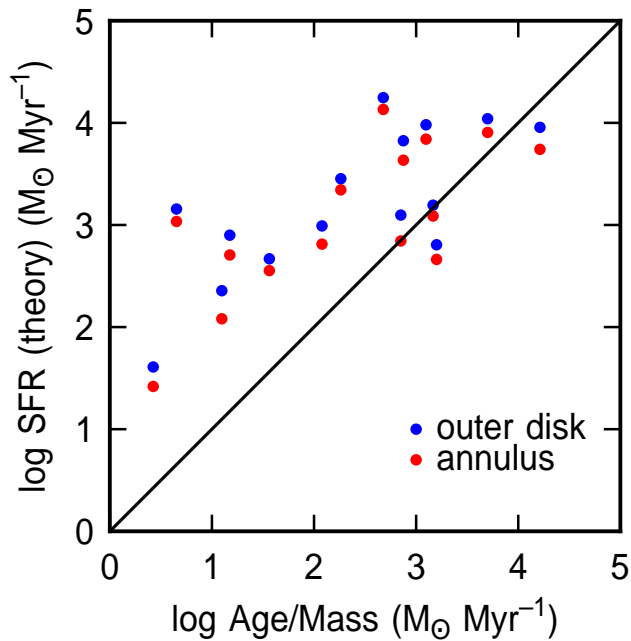


Fig. 12.— The theoretical star formation rates are plotted versus the average rate in the corresponding *FUV* knot. The blue points for the outer disk integral are slightly higher than the red points for an annulus around the knot. The line is the unity relation. The rates are equal for the largest knots, suggesting that star-forming regions like these could build up the outer disk. The smallest knots cannot account for the outer disks in their galaxies, but we could be missing similar knots because of faintness, or these particular knots could be uncharacteristically small for their galaxies.

are relatively thick compared to the radial extents (Hodge & Hitchcock 1966; van den Bergh 1988; Elmegreen & Hunter 2015), and the metallicities are ~ 8 times lower. Consequently, self-gravity is weak in the interstellar medium, cloud contraction times are long, ~ 100 Myr or more, and molecules are sparse. Moreover, the threshold column density for strong gravity inside clouds should be ~ 3 times lower than it is locally, placing this collapse threshold firmly in the optically thin regime where atomic gas should still dominate. Presumably molecules form after the collapse begins (Glover & Clark 2012; Krumholz 2012).

The star formation rates in the most remote *FUV* knots fall short by a factor of ~ 8 of the average rates obtained from the Kennicutt-Schmidt relation for these types of regions. Only for the most massive *FUV* knots are the rates comparable. Either we are missing other discrete star-forming regions owing to faintness or rapid dispersal, or the star formation rate drops below the KS relation for outer disks starting at around $\sim 1 M_{\odot} \text{ pc}^{-2}$. In the latter case, stellar scattering from the inner disk would have to fill the outer disks with stars, which go out much further than the last *FUV* knot seen here.

We are grateful to the Lowell Observatory Research Fund for funding, including a summer internship for EG. We are also grateful to John and Meg Menke for a donation to Lowell Observatory that covered part of the page charges and to IBM for covering the remainder. DAH also appreciates the considerable help on installing and running python to produce Figure 1 from Joe Llama (University of St. Andrews), Michael Mommert (NAU), and David Trilling (NAU). We appreciate helpful comments by the referee.

Facilities: GALEX

REFERENCES

- Ashley, T., Simpson, C. E., & Elmegreen, B. G. 2013, *AJ*, 146, 42
- Ashley, T., Elmegreen, B.G., Johnson, M., Nidever, D.L., Simpson, C.E., Pokhrel, N.R. 2014, *AJ*, 148, 130
- Bellazzini, M., Beccari, G., Fraternali, F., et al. 2014, *A&A*, 566, 44
- Bigiel, F., Leroy, A., Walter, F., Brinks, E., de Blok, W. J. G., Madore, B., & Thornley, M. D. 2008, *AJ*, 136, 2846
- Bigiel, F., Leroy, A., Walter, F., Blitz, L., Brinks, E., de Blok, W.J.G., Madore, B. 2010, *AJ*, 140, 1194

- Billett, O. H., Hunter, D. A., & Elmegreen, B. G. 2002, *AJ*, 123, 1454
- Burstein, D., & Heiles, C. 1984, *ApJS*, 54, 33
- Cannon, J. M., O’Leary, E. M., Weisz, D. R., et al. 2012, *ApJ*, 747, 122
- Cardelli, J. A., Clayton, G. C., & Mathis, J. S. 1989, *ApJ*, 345, 245
- Carraro, G., Villanova, S., Demarque, P., McSwain, M. V., Piotto, G., & Bedin, L. R. 2006, *ApJ*, 643, 1151
- de Blok, W. J. G., & Walter, F. 2000, *ApJ*, 537, L95
- de Blok, W. J. G., Walter, F., Brinks, E., Trachternach, C., Oh, S.-H., & Kennicutt, R. C., Jr. 2008, *AJ*, 136, 2648
- Elmegreen, B.G. 2015, *ApJ*, 814, L30
- Elmegreen, B.G., & Struck, C., 2013, *ApJ*, 775, L35
- Elmegreen, B. G., & Hunter, D. A. 2015, *ApJ*, 805, 145
- Elmegreen, D.M., Elmegreen, B.G., Sánchez Almeida, J., Muñoz-Tuñón, C., Mendez-Abreu, J., Gallagher, J.S. Rafelski, M., Filho, M., & Ceverino, D. 2016, *ApJ*, submitted
- Glover, S.C.O. & Clark, P.C. 2012, *MNRAS*, 421, 9
- Herrmann, K. A., Hunter, D. A., & Elmegreen, B. G. 2013, *AJ*, 146, 104
- Hodge, P. W., & Hitchcock, J. L. 1966, *PASP*, 78, 7
- Hunter, D. A., & Elmegreen, B. G. 2004, *AJ*, 128, 2170
- Hunter, D. A., & Elmegreen, B. G. 2006, *ApJS*, 162, 49
- Hunter, D. A., Elmegreen, B. G., Dupuy, T. J., & Mortonson, M. 2003, *AJ*, 126, 1836
- Hunter, D. A., Elmegreen, B. G., & Ludka, B. C. 2010, *AJ*, 139, 447
- Hunter, D. A., Elmegreen, B. G., Oh, S.-H., et al. 2011, *AJ*, 142, 121
- Hunter, D. A., Ficut-Vicas, D., Ashley, T., et al. 2012, *AJ*, 144, 134
- Kennicutt, R. C., Jr. 1989, *ApJ*, 344, 685
- Kennicutt R. C., & Evans N. J., 2012, *ARA&A*, 50, 531

- Komiyama, Y., Okamura, S., Yagi, M., et al. 2003, *ApJ*, 590, L17
- Krumholz, M.R. 2012, *ApJ*, 759, 9
- Lada, C.J., Lombardi, M., & Alves, J.F. 2010, *ApJ*, 724, 687
- Landolt, A. U. 1992, *AJ*, 104, 340
- Leitherer, C., Schaerer, D., Goldader, J. D., et al. 1999, *ApJS*, 123, 3
- Martin, D. C., Fansom, J., Schiminovich, D., et al. 2005, *ApJ*, 619, L1
- Martín-Navarro, I., Trujillo, I., Knapen, J.H., Bakos, J., Fliri, J. 52 2014, *MNRAS*, 441, 2809
- Melena, N. W., Elmegreen, B. G., Hunter, D. A., & Zernow, L. 2009, *AJ*, 138, 1203
- Minchev, I., Famaey, B., Quillen, A. C., Di Matteo, P., Combes, F., Vlajic, M., Erwin, P., Bland-Hawthorn, J. 2012, *A&A*, 548, A126
- Nidever, D., Ashley, T., Slater, C. T., et al. 2013, *ApJL*, 779, L15
- Oh, S.-H., Hunter, D. A., Brinks, E., et al. 2015, *AJ*, 149, 180
- Padoan, P., Haugbølle, T., Nordlund, Å., 2012, *ApJ*, 759, L27
-] Pellerin, A., Meyer, M., Harris, J., & Calzetti, D. 2008, *ASPC*, 388, 379
- Radburn-Smith, D. J., Roškar, R., Debattista, V. P., et al. 2012, *ApJ*, 753, 138
- Roškar, R., Debattista, V. P., Quinn, T. R., Stinson, G. S., & Wadsley, J. 2008, *ApJ*, 684, L79a
- Rubio, M., Elmegreen, B.G., Hunter, D.A., Brinks, E., Cortés, J.R., & Cigan, P. 2015, *Nature*, 525, 218
- Saha, A., Olszewski, E. W., Brondel, B.
- Sánchez Almeida, J., Muñoz-Tuñón, C. Elmegreen, D., Elmegreen, B., & Mendez-Abreu, J. 2013, *ApJ*, 767, 74
- Sánchez Almeida, J. Morales-Luis, A.B., Muñoz-Tuñón, C., Elmegreen, D.M., Elmegreen B.G., & Mendez-Abreu, J. 2014a, *ApJ*, 783, 45

- Sánchez Almeida, J. Elmegreen, B.G., Munoz-Tunon, C., Elmegreen D.M., Perez-Montero, E., Amorin, R., Filho, M.E., Ascasibar, Y., Papaderos, P., & Vilchez, J.M. 2015, ApJL, 810L, 15
- Salpeter, E. E. 1955, ApJ, 121, 161
- Toomre, A. 1964, ApJ, 139, 1217
- van den Bergh, S. 1988, PASP, 100, 344
- Walter, F., Brinks, E., de Blok, W. J. G., et al. 2008, AJ, 136, 2563
- Wang, J., Fu, J., Aumer, M., Kauffmann, G., Józsa, G.I.G., Serra, P., Huang, M.-l., Brinchmann, J., van der Hulst, T., Bigiel, F. 2014 MNRAS, 441, 2159
- Wyder, T. K., et al. 2007, ApJS, 173, 293
- Zhang, H.-X., Hunter, D. A., Elmegreen, B. G., Gao, Y., & Schrubba, A. 2012, AJ, 143, 47